GEOPERSIA

Accepted Manuscript

Efficient Estimation of Shear Strength Parameters of Unsaturated Soils Through Artificial Neural Networks

Habib Rahimimanbar, Gholamreza Shoaei, Mohammad Fathollahy

DOI: 10.22059/geope.2026.404511.648848

Receive Date: 19 October 2025
Revise Date: 22 December 2025
Accept Date: 20 January 2026

Efficient Estimation of Shear Strength Parameters of Unsaturated Soils Through Artificial Neural Networks

Habib Rahimimanbar [1], Gholamreza Shoaei [1], *, Mohammad Fathollahy [2]

[1] Department of Geology, Engineering Geology Group, Faculty of Basic Sciences, Tarbiat Modares University, Iran
[2] Department of Geology, Faculty of Basic Sciences, Kurdistan University, Iran

Received: 19 October 2025, Revised: 22 December 2025, Accepted: 20 January 2026

Abstract
Laboratory testing of unsaturated soil shear strength parameters is often time-consuming, expensive, and requires specialized equipment. This study explores Artificial Neural Networks (ANNs) as an alternative, systematically optimizing the predictive model through a novel, multi-stage analysis investigating activation functions and iteratively tuning hidden layer counts and neuron numbers. A comprehensive evaluation of 195 network configurations was conducted using a dataset of 490 points compiled from 14 soil types, primarily fine-grained soils. Modeling identified the Bayesian regularization (TRAIN BR) function as superior (R=0.97). Subsequent expansion to three, four, and five hidden layers (with neuron counts from 50 down to 10) determined the most effective architecture. The four-layer Multilayer Perceptron (MLP) network emerged as the optimal configuration, achieving exceptional performance with an overall R^2 value of 0.98. Model validation utilized rigorous approaches. Initially, reserved samples confirmed the four-layer network's high accuracy for cohesion. Secondly, predictions were compared with established empirical methods, demonstrating significantly higher accuracy. Finally, five independently prepared samples tested via in-house Direct Shear Testing further validated the model's reliability. This external validation confirmed close agreement, showing prediction errors ranging from 1% to 11% for friction angle and 3% to 14% for cohesion. While further validation using a wider diversity of soil types and a larger external sample size is required to confirm generalizability, these results firmly establish ANNs as a powerful, accurate, and cost-effective tool for geotechnical engineers providing reliable estimates of unsaturated soil shear strength parameters.

Keywords: ANN-Based Modeling of Unsaturated Soils, Shear Strength Prediction, Cohesion and Friction Angle Estimation, Soil Suction, MLP Architecture Optimization.

Introduction

Many soils in nature exist in an unsaturated state (Fredlund et al., 1993). In arid and semi-arid regions, unsaturated soils are commonly found in environments with low relative humidity, resulting in very high suction values, often reaching 10 or even 100 MPa (Gao et al., 2020).
Shear strength is a critical engineering property that plays a vital role in the design of many geotechnical and geo-environmental structures, including pavements, earth embankments, retaining walls, covers, and liners. This property determines a material's ability to resist forces that cause sliding or shearing along a surface (Vanapalli et al., 2000). Fundamentally, it represents the maximum shear stress that soil can withstand before failure occurs and is one of the most important parameters in geotechnical engineering.

While the Mohr–Coulomb equation is widely used to describe the shear behavior of saturated

* Corresponding author e-mail: shoaei@modares.ac.ir

soils (Johnson et al., 1987), determining the shear strength of unsaturated materials **is** inherently more complex. To address this, Fredlund et al. (1978) proposed a linear equation specifically for the shear strength of such soils:

$$\tau_f = c' + (\sigma - u_a)_f tan\varphi' + (u_a + u_w)_f \, tan\emptyset_b \quad (1)$$

where τf (kPa) is the unsaturated shear strength, c′ (kPa) and ϕ′ are the effective cohesion and effective friction angles, respectively, (σ−ua) (kPa) is the net normal stress at the failure plane at failure, (ua+uw) (kPa) is the matric suction at failure, σ is the total normal stress, ua and uw are the pore-air and pore-water pressures, respectively. ϕb is an angle that indicates the rate of change of strength relative to changes in matric suction (Fredlund et al., 1978).

The total or apparent cohesion (c) ofthis soils therefore consists of two components: c′ from physicochemical cohesion and a component from matric suction (Zhang et al., 2001) expressed as:

$$c = c' + (u_a + u_w)tan\emptyset_b \quad (2)$$

Although Fredlund et al. (1978) proposed a linear equation, many experimental results show that the relationship between strength and soil suction is actually nonlinear (Gan et al., 1988). Figure 1 illustrates the failure envelope related to matric suction and shows how friction angle ($'$) and cohesion (c') relate to variations in shear strength and matric suction. The friction angle and cohesion are typically assumed to match those obtained from saturated soil tests under low suction/near-saturation conditions (Fredlund et al., 2011) The failure envelope associated with matric suction generally consists of two parts: a linear portion up to the air entry value where the soil remains saturated, and a nonlinear portion where desaturation begins. Within the range of matric suction typically applied in triaxial testing, the nonlinearity of the failure envelope is closely associated with the air entry value (AEV). The AEV can vary with the applied normal stress because increasing normal stress tends to compress soil pores and reduce the size of air-filled voids, thereby requiring higher suction for air to enter the pore space (Rassam et al., 1999).

Since the 1970, researchers have proposed various forms of unsaturated shear strength equations (Bao et al., 1998). However, many of these equations are difficult to apply in practice. Therefore, a simpler methodology based on readily available soil properties is needed. The strength of such soils is governed by several factors, including soil type, grain size distribution, density, and stress state (Vanapalli et al., 2009). Matric suction is a fundamental parameter influencing this behavior and is considered a component of cohesion (Likos et al.,2019). Early investigations at Imperial College, London (Bishop et al 1960) suggested that strength may be correlated with the degree of soil saturation. Several equations have been proposed to represent the soil water characteristic curve (SWCC) 0 Fredlund et al., 1994). Rassam and Williams developed a predictive function expressing strength in terms of matric suction and normal stress based on three-dimensional nonlinear regression analysis (Rassam et al., 1999). Soil type, particularly grain size distribution and soil texture, is a critical factor affecting this property (Gao et al., 2020). Gao et al. (2020) demonstrated that different soil types exhibit distinct suction ranges (e.g., 0-10 kPa for fine sand and 0-100 MPa for clay) and display different strength behaviors. Marinho and Oliveira (2012) established that the mechanical response of such soils is related to soil water retention characteristics and Atterberg limits (Marinho et al., 2022). The grain size distribution curve can also be utilized to estimate the SWCC for these materials. The SWCC is a fundamental property of unsaturated soils that characterizes the relationship between soil water content and soil suction (Fredlund et al., 2011). The SWCC is also influenced by Atterberg limits, and its parameters can be correlated with various soil properties (Chai et al., 2020; Perera et al., 2005; Zhang et al., 2018). Fredlund (2019) suggested that the slope of the unsaturated strength envelope remains equal to the tangent of the soil's internal friction angle up to the air entry value (AEV) (Fredlund et al., 2018). As clay soils dry from initial water contents above the liquid limit, they typically exhibit

a gradual increase in strength. Atkinson (2007) reported that at the liquid limit it reaches approximately 1.7 kPa, whereas Wood (1990) suggested that the average effective stress in the soil at the same state is about 8 kPa (Figure 2). Although the resistance is relatively low at the liquid limit, the soil still experiences compression, increasing its effective stress. As drying continues and pore water pressure decreases, matric suction and effective stress both rises, leading to a pronounced increase in strength and stiffness. Most soils desaturate as their water content approaches the plastic limit. For clayey soils, the strength at this limit is about 170 kPa–roughly two orders of magnitude higher than at the liquid limit. As water content decreases below the plastic limit, volume reduction slows while resistance to shearing increases considerably. When the material reaches zero water content, suction may approach 106 kPa. Therefore, a significant increase in strength occurs between the liquid and plastic limits of clayey soils, reflecting a complex interaction among water content, volume change, and mechanical response (. Shear resistance is also governed by net normal stress (Abd et al., 2020). Figure 2 illustrates the projections of peak failure envelopes in the matric suction–shear stress plane for direct shear tests on unsaturated materials at varying net normal stress levels. Zhou et al. (2016) demonstrated a significant increase in strength with greater net normal stress or matric suction [28]. Various experimental methods have been employed to measure this parameter, including shear vane tests, torsional shear appear Fredlund et al., 2011). atus, drop-cone penetrometers, direct shear boxes, Zhang's (2001) method, in-situ shear boxes, and triaxial testing; however, most are complex and time-consuming, which limits large-scale application (Khaboushan et al., 2018).

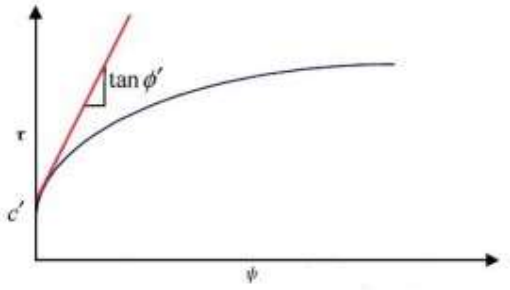

Figure 1. Relationship between shear strength and matric suction

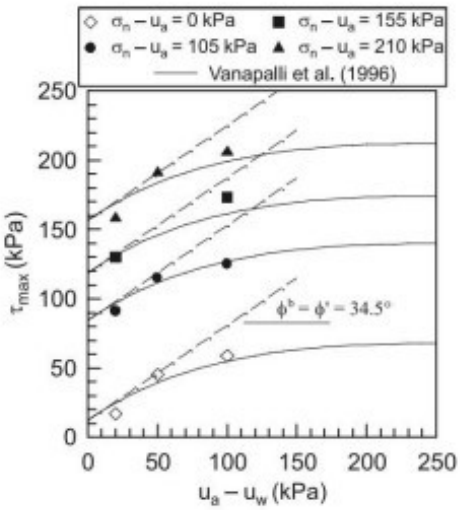

Figure 2. Peak failure envelope projections in the matric suction-shear stress plane for unsaturated soil direct shear tests at varying net normal stresses

This property is influenced by a complex interplay of several intrinsic and extrinsic parameters, demanding rigorous empirical and theoretical documentation. Key among these are soil type and grain size distribution curves, which have been critically investigated by Fredlund and colleagues (2011, 2012). Furthermore, soil water retention characteristics–specifically Atterberg limits–directly impact the matric suction component of strength (Marinho et al., 2012). Recent studies have also highlighted fundamental properties like specific gravity (Gs) (Das et al., 2021), along with the established effect of net normal stress on mobilizing shear resistance (Zhou et al., 2016). The varying response across different soil matrices underscores the necessity of establishing reliable relationships for each dominant factor, as demonstrated by the work on soil type effects (Gao et al., 2020) (Gao et al., 2020; Fredlund et al., 2011; Marinho et al., 2012; Fredlund et al .,2019; Das et al., 2021; Gao et al., 2020).

Conventional experimental and empirical approaches have provided valuable insights into this mechanical response; however, these methods often require extensive laboratory testing and may not efficiently capture the complex, nonlinear interactions among multiple influencing factors.

In this context, the growing field of computational intelligence offers an effective alternative for dealing with such complexities. In recent years, computational intelligence methods have shown remarkable progress in solving engineering problems that are difficult to address using traditional techniques. The fundamental principle behind these methods is to identify hidden relationships among different datasets and to apply this learned knowledge to new situations. 0Churchland et al., 1992). Lee et al. (2003) formulated a nonlinear relationship between resistance and matric suction in hyperbolic form and developed a method to predict maximum cohesion (C_{max}) using an artificial neural network (ANN) (Lee et al., 2003). Khaboushan et al. (2018) employed multiple linear regression (MLR) to to estimate shear parameters, including effective cohesion (c'), effective internal friction angle (φ'), and the internal friction angle related to matric suction (φ^b). The input parameters included particle size distribution (sand, silt, and clay percentages or geometric mean diameter, dg, and geometric standard deviation, σg), organic matter (OM) content, calcium carbonate (CaCO3) content, compactness indices (bulk density, ρb, and relative bulk density, ρb-rel), mean weight diameter of aggregates (γ_{dry}, γ_{wet}), and structural stability indices (aggregate stability, AS, stability index, SI, and crusting index, Ic). Their findings indicated that φb showed no significant correlation with soil properties, suggesting that φb is primarily influenced by matric suction rather than soil properties. Clay, coarse sand (CS), and very fine sand (VFS) were incorporated in the model to predict c', while pedotransfer functions (PTFs) using fine sand (FS) and VFS as predictors could accurately estimate φ' (Khaboushan et al.,2018). However, many of these parameters are not commonly available in standard geotechnical practice. Therefore, there is a need to develop prediction methods based on readily available geotechnical parameters. Based on the preceding discussion, it can be concluded that the shear behavior of such soils can be predicted using commonly available soil properties such as specific gravity (Gs), percentages of sand, silt, and clay, degree of saturation (Sr), dry unit weight (γd), liquid limit (LL), plastic limit (PL), plasticity index (PI), net normal stress (σ3-ua), and conventional shear strength parameters (c' and φ') through neural network analysis. This approach can significantly reduce the need for additional specialized testing such as unsaturated shear strength or soil water characteristic curve (SWCC) tests; however, laboratory verification remains essential to ensure the reliability and applicability of the predicted results.

This study aimed to develop a cost-effective and accurate predictive model for unsaturated soil shear strength using Artificial Neural Networks (ANNs), trained on a comprehensive dataset from literature. The novel methodology involved optimizing network architecture and training functions to identify the most effective configuration. A key distinguishing feature of

this research is its rigorous external validation, which included in-house Direct Shear Testing on independent soil samples to confirm the model's practical applicability.

Materials and methods

Data collection

Training an artificial neural network requires an appropriate collection of information. A suitable compilation should consist of reliable and accurate, contain a sufficient number of data points to ensure accurate results, and cover all relevant aspects of the problem (Baziar et al.,2005). As previously mentioned, laboratory measurements of unsaturated soil shear strength are time-consuming and require expensive equipment. Therefore, conducting laboratory tests specifically to train a neural network may not be cost-effective. In this study, a suitable information base for training the neural network was compiled from published literature (Gan et al., 1988; Alzaidy et al.,2018; Thu et al., 2007).

First, the initial pool of data was filtered based on recognized laboratory testing standards (such as ASTM/ISO) to minimize bias from differing testing protocols. All data were then converted to a consistent unit system. Additionally, statistical checks–including assessments of multicollinearity, distribution skewness, and potential outliers–were performed prior to ANN training to ensure data integrity and model reliability.

Outlier Filtering and Justification of 490 Data Points:

Following this initial methodological standardization, we then proceeded to a crucial second step: identifying and removing data points that appeared unreasonable, illogical, or fell outside physical limitations (acting as significant outliers). It was only after this rigorous filtering of non-physical and inconsistent data that our final dataset size was established at exactly 490 independent data points. A total of 490 points were collected from 14 different soil types. The soils were classified according to both the Unified Soil Classification System (USCS) and the USDA Soil Taxonomy Classification, and numerical values were assigned to each classification. For the USDA soil taxonomy classification, soils were labeled based on particle size, ranging from small to large. For the USCS classification, soils were labeled based on both plasticity index and particle size, ranging from low to high. Only soils with identifiable Atterberg limits were included in the study. Table 1 presents the 14 soil types from which observations were collected, along with their respective classifications and designations.

Table 1. Soil types with USCS (Unified Soil Classification System) and USDA (United States Department of Agriculture, soil classification system) classifications and their assigned numerical labels

Count	USCS	Label	USDA	Label
1	MH	4	Clay Loam	4
2	CL	2	Clay	1
3	CL	2	Loam	8
4	CL	2	Silty Clay Loam	3
5	CH	1	Silty Clay	2
6	CL	2	Silty Clay Loam	3
7	CH	1	Silty Clay	2
8	CL	2	Clay Loam	4
9	CH	1	Clay	1
10	CL	2	Silty Clay Loam	3
11	CL	2	Silty Clay Loam	3
12	SM-SC	7	Sandy Loam	10
13	CL	2	Clay Loam	4
14	SC	6	Loamy Sand	11

Data Normalization

Normalization of the data prior to training a neural network can contribute to improved convergence, accuracy, stability, and proper data behavior (Ioffe & Szegedy, 2015). A common normalization technique is Max-Min Scaling, which scales the features of a dataset into a specific range, typically between 0 and 1. In this study, the dataset was scaled using this method to the range of zero to one. Equation 1 illustrates the Min-Max scaling method:

$$x\ scaled = \frac{X - X_{min}}{X_{max\_}X_{min}} \quad (3)$$

In this equation, X scaled represents the normalized value, X is the original value, X min is the minimum value of the data in a column, and X max is the maximum value of the data in a column.

After network prediction, the scaled output values were inversely transformed to recover the original physical units (kPa) using the corresponding Min–Max parameters.

Statistical analysis

Statistical descriptions of the collected data are presented in Table 2. Heatmaps are useful visualization tools for identifying patterns and relationships in large datasets (Wilke et al., 2019). Figure 3 shows the Seaborn heatmap of the dataset. This heatmap displays a matrix of color-coded values representing the correlations between variables in the dataset. The color of each cell indicates the strength and direction of the correlation, with warmer colors representing positive correlations and cooler colors representing negative correlations. The correlation coefficient is a statistical measure that quantifies the strength and direction of the linear relationship between two variables (Myers et al., 2014). The coefficient ranges from -1 to 1, where -1 indicates a perfect negative correlation, 1 indicates a perfect positive correlation, and 0 indicates no correlation. Normalizing the dataset before training a neural network can improve convergence, accuracy, stability, and feature treatment while enabling more effective regularization (Ioffe et al., 2015). A commonly used normalization method is the min-max scaler, which maps dataset features to a specific range, typically between 0 and 1. In this study, both the input variables and target variables were scaled using the min-max scaler to fall within the range of 0 to 1.

Table 2. Descriptive statistics of input and output parameters for the collected dataset

In or output data	Statistics	Count	Mean	Std	Min	0.25	0.5	0.75	Max
Out put	Gs	490	2.68	0.04	2.61	2.66	2.68	2.72	2.73
	%C	490	32.52	16.66	4	24	30	42	72
	%M	490	40.34	13.21	11	27	44	48	61
	%S	490	27.14	23.1	1	9.5	23	49	85
	%LL	490	40.15	14.89	22	31	36	47	71.1
	%PL	490	23.13	7.52	10	17	19.4	29	36.5
	PI	490	17.02	8.33	6	10	18	20.5	35
	γ_d(KN/m^3)	490	16.38	1.72	12.93	15.5	16.75	17.72	18.4
	бn-Ua (kPa)	490	87.47	51.52	0	50	100	120	200
	USDA	490	4.54	3.3	1	2	3	8	11
	USCS	490	2.84	2.06	1	2	2	4	7
In put	C'	490	23.28	22.1	0	5	20	28.1	82
	Φ'	490	31.29	4.79	23	28	32	34	40
In put	Ψ(kPa)	490	1132.78	2774.6	0.04	110.88	253.34	594.76	15000
Out put	τ(kPa)	490	182.36	192.9	1.15	83.85	104.35	175.28	1207.08

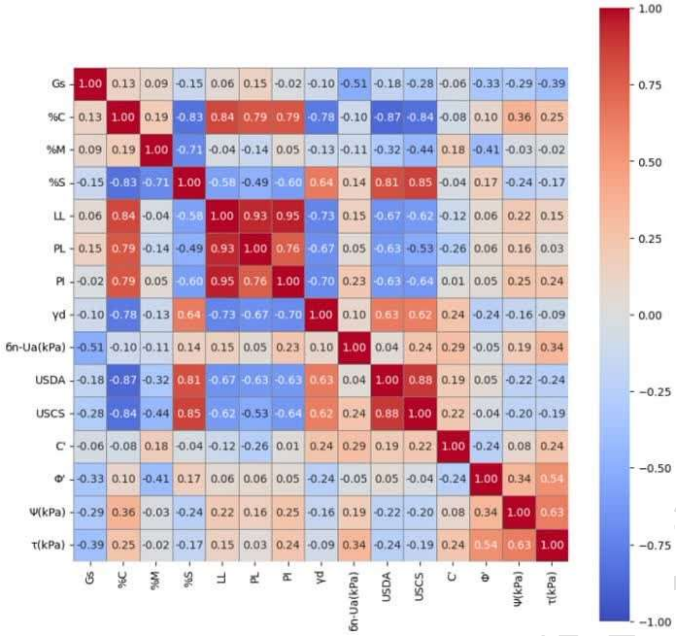

Figure 3. Seaborn heatmap of dataset showing a matrix of color-coded values that represent the correlation between variables in the dataset

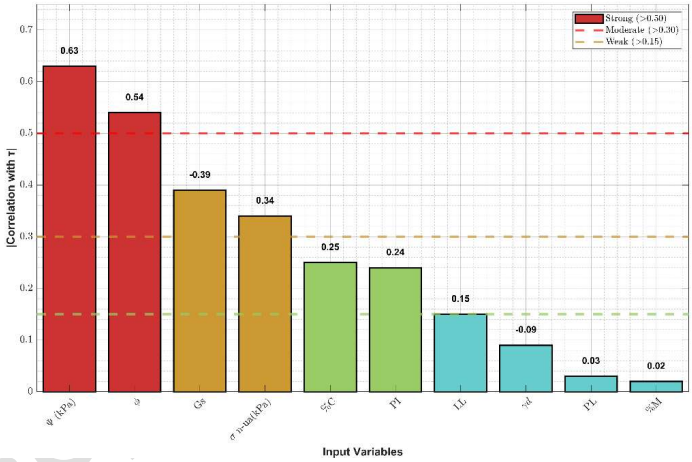

Figure 4. Feature Importance Ranking for Shear Strength Prediction Based on Correlation Analysis

The predictive power of the model inputs was quantified using correlation analysis against the target variable (τ). This analysis reveals that matric suction (ψ) and effective friction angle (ϕ′) exhibit the strongest positive correlations (r=0. and r=0.54 respectively), clearly indicating they encode the primary physical mechanisms governing shear behavior in unsaturated materials. In contrast, several input variables, such as the plastic limit (PL, r=0.03) and silt content (%M, r=0.02), demonstrated correlations near zero, justifying their exclusion from the input layer to optimize model complexity and focus learning on the most discriminative features.

We used the Garsen score used to determine the relative importance of input variables. The Garsen score measures the importance of input features by evaluating the impact of removing each feature on the performance of the neural network. The score is based on the difference between the error (or loss) of the model when all features are used and the error of the model when a specific feature is removed 0 Ioffe et al., 2015). The larger the difference in error, the more important the feature is considered to be. The Garsen score results indicate that particle size and Φ' has a significant impact on shear strength.

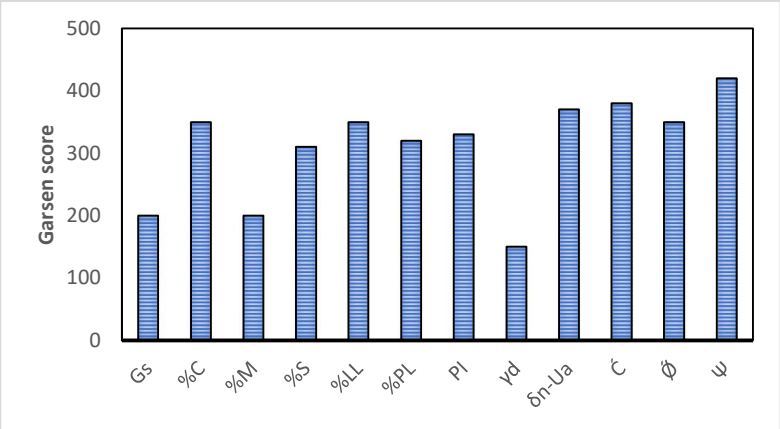

Figure 5. The Garsen score to determine the relative importance of input variables

Neural network modeling

A neural network is a type of machine-learning algorithm that is modeled after the structure of the human brain 0. It consists of multiple interconnected layers of nodes, called neurons, that work together to process data and make predictions. Each neuron receives input from other neurons in the previous layer and produces an output, which is then passed on to the next layer 0 Rosenblatt et al., 1958).

Neural network structure for the given problem

This study employed feedforward neural network (FF) and multilayer perceptron (MLP) architectures for data analysis. The number of hidden layer nodes and the number of hidden layers were determined through trial and error. The optimal number of neurons and hidden layers is achieved when the network produces the best performance 0 Rosenblatt et al., 1958) and the optimal network structure was determined through iterative experiments combined with Early Stopping. Accordingly, neural networks with one, two, three, four, and five hidden layers were evaluated, with neuron counts of 10, 20, 30, 40, and 50 tested for each configuration. A total of 195 networks were trained and evaluated, comprising 84 single-layer networks, 84 two-layer networks, 7 three-layer networks, 10 four-layer networks, and 10 five-layer networks (Table 3 and Figures 7 and 8).

Activation Function Selection: Initially, we evaluated all potential activation functions using single-layer and two-layer architectures to identify the most effective activation function for predicting the shear strength parameters.

Impact of Layer Depth: Once the optimal activation function was established, we then investigated the impact of increasing network depth, specifically testing 3, 4, and 5 hidden layers.

Neuron Count Optimization: Finally, maintaining the optimal layer count and activation functions determined in the preceding steps, we optimized the network width by systematically evaluating uniform neuron counts of 50, 40, 30, 20, and 10 within each hidden layer for the best-performing depths. All the steps mentioned in Figure 5 are shown concisely.

To identify the optimal network configuration, the analysis was conducted in stages. Initially, single-layer and two-layer networks were trained with 10 neurons in the hidden layer. Subsequently, based on the best-performing configurations from the initial stage, networks with 3, 4, and 5 hidden layers were evaluated using varying neuron counts of 50, 40, 30, 20, and 10 in each hidden layer (Architectures were systematically evaluated using a uniform neuron count (ranging from 10 to 50) across all hidden layers, rather than testing all possible permutations between layers).

Table 3. Number of processed neural network with different layers

Number of Layers	Number of networks
One layers	84
two Layers	84
three layers	7
four layers	10
five layers	10
Total	195

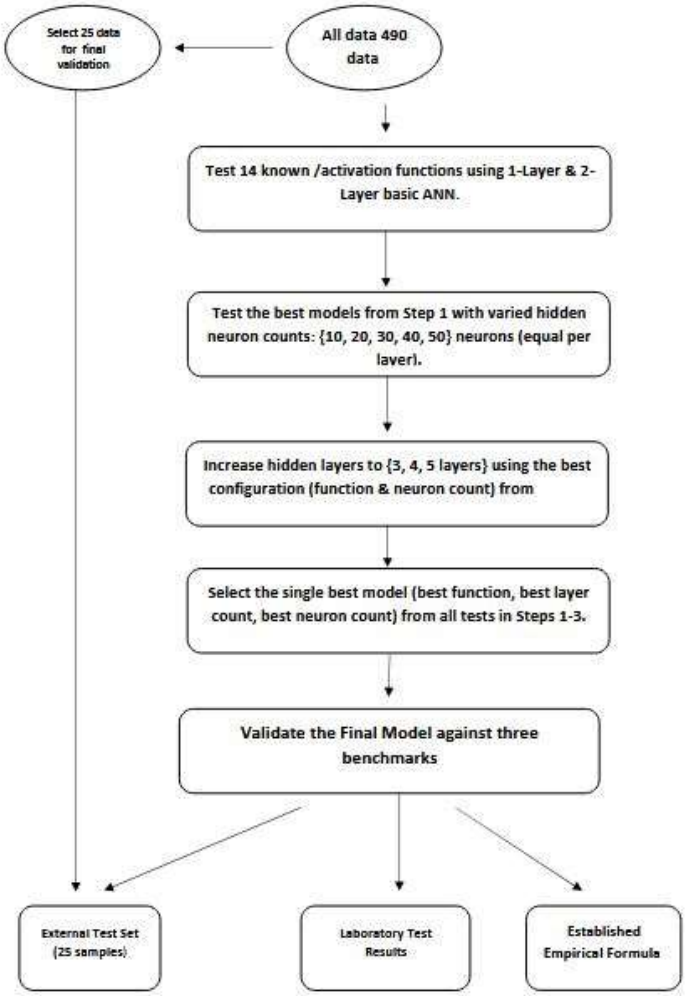

Figure 6. Systematic protocol for ANN architecture Selection and validation.

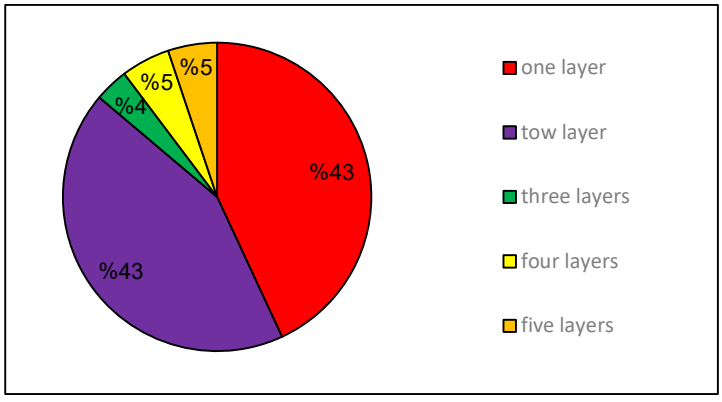

Figure 7. Distribution of trained neural networks by number of hidden layers

learning process

The training process involves iterative cycles of forward propagation to calculate the output, followed by backpropagation to compute the error gradient and adjust the network weights accordingly, which constitutes a single learning step.

This study evaluated 14 different training functions for the neural networks. The number of networks trained with each function is presented in Figure 9 and Table 4.

In this study, 14 different well-known training algorithms available in the MATLAB environment were systematically evaluated to identify the most efficient and robust configuration for the Artificial Neural Network (ANN) when applied to the prediction of shear strength parameters of unsaturated soils. Dataset splitting, and the number and processing of neural networks trained with each of these functions can be seen in Figure 8

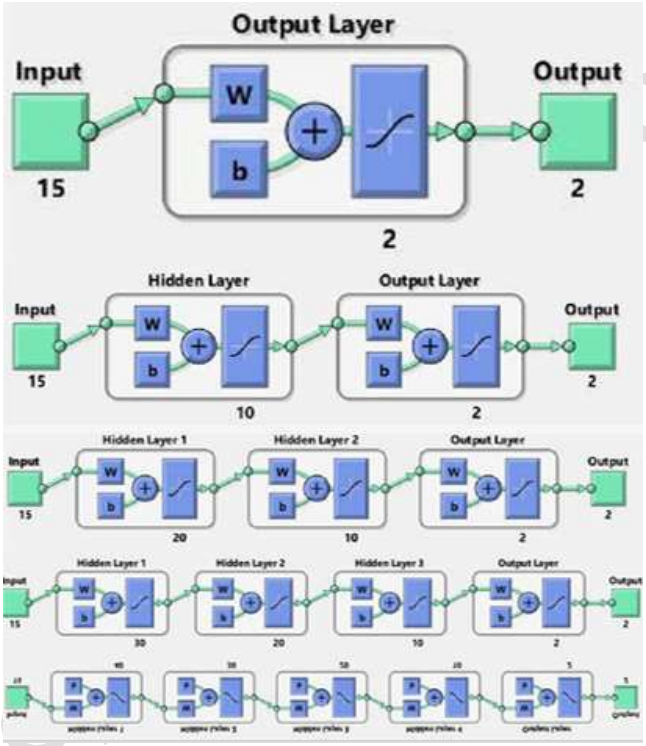

Figure 8. Shows the number of hidden layers from one to five hidden layers in order from top to bottom

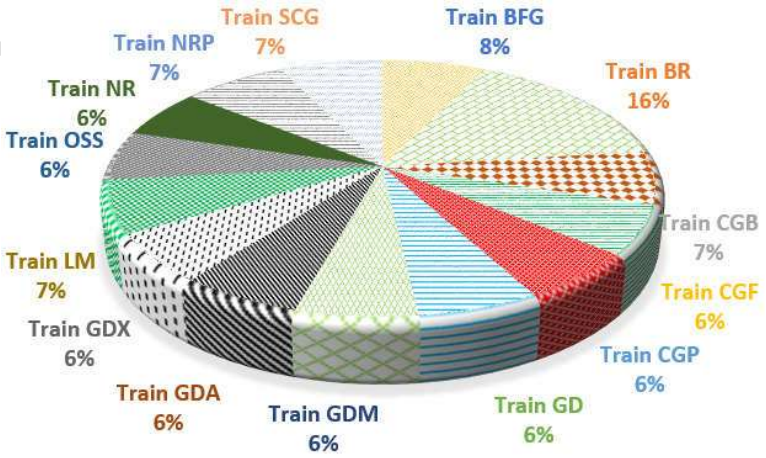

Figure 9. Distribution of trained neural networks by training function

In this study, 5% of the total dataset for model validation, (25 out of 490 samples) including both input and output parameters were initially separated and reserved for final validation (data shown in Tables 8 and 9). The remaining dataset was divided such that 70% was used for training the neural networks and 30% was used for testing. Three performance learning functions were evaluated: 77 networks were trained with the mean squared error (MSE) learning function, 59 networks with the mean squared error with regularization (MSE REG) learning function, where for the regularization term a penalty term is used to encourage the network to use simpler, and more generalizable weight. Moreover, 59 networks with the standard error of the estimate (SEE) learning function (Figure 10 and Table 5). SSE is calculated as the square root of the residual variance, which makes it directly related to the MSE (which is the mean of the squared errors). Additionally, two adaptive learning functions were implemented: 90 networks utilized the gradient descent (GD) adaptive learning function and 105 networks utilized the gradient descent with momentum (GDM) adaptive learning function (Figure 10 and Table 6).

Table 4. Number of trained neural networks for each training function.

Row	Educational function	Number
1	Train BFG	14
2	Train BR	31
3	Train CGB	13
4	Train CGF	12
5	Train CGP	12
6	Train GD	12
7	Train GDM	12
8	Train GDA	12
9	Train GDX	12
10	Train LM	13
11	Train OSS	12
12	Train NR	12
13	Train NRP	14
14	Train SCG	14
	Total	195

Table 5. Number of trained neural networks for each performance learning function

Row	Adaptive Learning function	Number
1	MSE	77
2	MSE REG	59
3	SEE	59
	Total	195

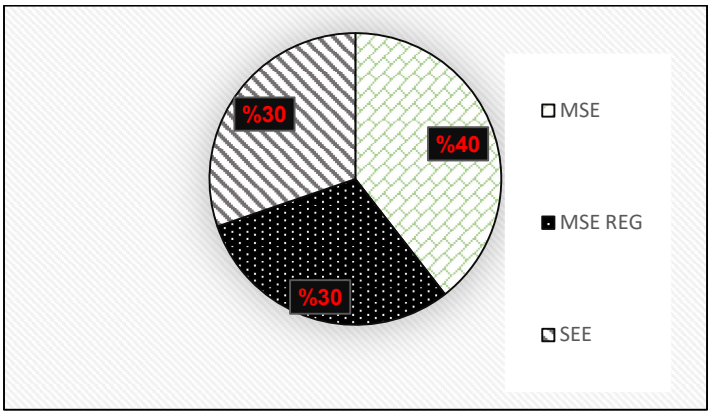

Figure 10. Distribution of trained neural networks by performance learning function

77 networks were processed with the MSE learning function, 59 networks were processed with the MSE REG learning function, and 59 networks were processed with the SEE learning function.

Interpretation of neural network results

Table 6 presents the best-performing single-layer and double-layer neural networks, labeled a through m. Among the optimal configurations, the Train BR training function showed the highest frequency. The MSE performance learning function was used in 6 cases, while the Learn GD adaptive learning function demonstrated the highest frequency. Therefore, Train BR, MSE, and Learn GD were identified as the most effective training function, performance learning function, and adaptive learning function, respectively, for this problem. Subsequently, networks with three, four, and five hidden layers were evaluated by varying the number of neurons in the hidden layers while utilizing these optimal functions. Table 7 presents the five best-performing networks using the optimal functions, labeled n through r. The architectures of these networks are illustrated in Figure 12.

Table 6. Number of trained neural networks for each adaptive learning function.

Row	Adaptive learning functions	Number
1	Learn GD	90
2	Learn GDM	105
	Total	195

Table 7. Performance of optimal neural network configurations with one through five hidden layers.

R All	R Test	R The accuracy of education	R Education	Transfer function	Number of layers	Operative learning function	function Adaptive learning	Training function	Name
0.97	0.96	0.97	0.96	TAN SIG	2	SEE	Learn GD	Train BFG	a
0.97	0.96	0.95	0.97	TAN SIG	2	MSE	Learn GDM	Train BFG	b
0.97	0.95	-	0.95	TAN SIG	1	SEE	Learn GD	TRAIN BR	c
0.97	0.95	-	0.95	TAN SIG	1	MSE	Learn GDM	TRAIN BR	d
0.97	0.84	-	0.99	TAN SIG	2	MSE	Learn GD	TRAIN BR	e
0.97	0.82	-	0.99	TAN SIG	2	SEE	Learn GD	TRAIN BR	f
0.97	0.83	-	1	TAN SIG	2	MSE	Learn GDM	TRAIN BR	g
0.97	0.95	-	0.97	TAN SIG	2	MSE REG	Learn GDM	TRAIN BR	h
0.97	0.97	0.98	0.96	TAN SIG	2	MSE	Learn GD	TRAIN CGB	i
0.97	0.96	0.95	0.97	TAN SIG	2	MSE	Learn GDM	TRAIN LM	j
0.97	0.97	0.98	0.96	TAN SIG	2	MSE REG	Learn GDM	TRAIN NRP	k
0.97	0.99	0.93	0.97	TAN SIG	2	MSE	Learn GD	TRAIN SCG	l
0.97	0.96	0.97	0.96	TAN SIG	2	MSE	Learn GDM	TRAIN SCG	m
	0.97	0.97	0.96	TAN SIG	1	MSE	Learn GDM	TRAIN BR	n
	0.95	0.74	1	TAN SIG	2	MSE	Learn GDM	TRAIN BR	o
	0.98	0.87	1	TAN SIG	3	MSE	Learn GDM	TRAIN BR	p
	0.98	0.90	1	TAN SIG	4	MSE	Learn GDM	TRAIN BR	q
	0.97	0.81	0.99	TAN SIG	5	MSE	Learn GDM	TRAIN BR	r

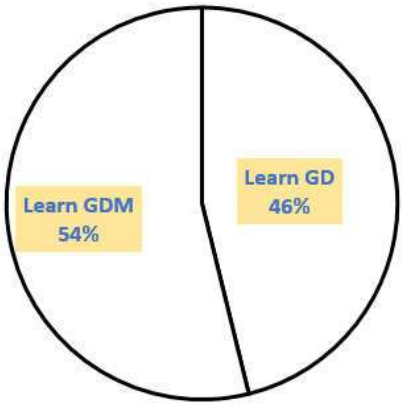

Figure 11. Distribution of trained neural networks by adaptive learning function

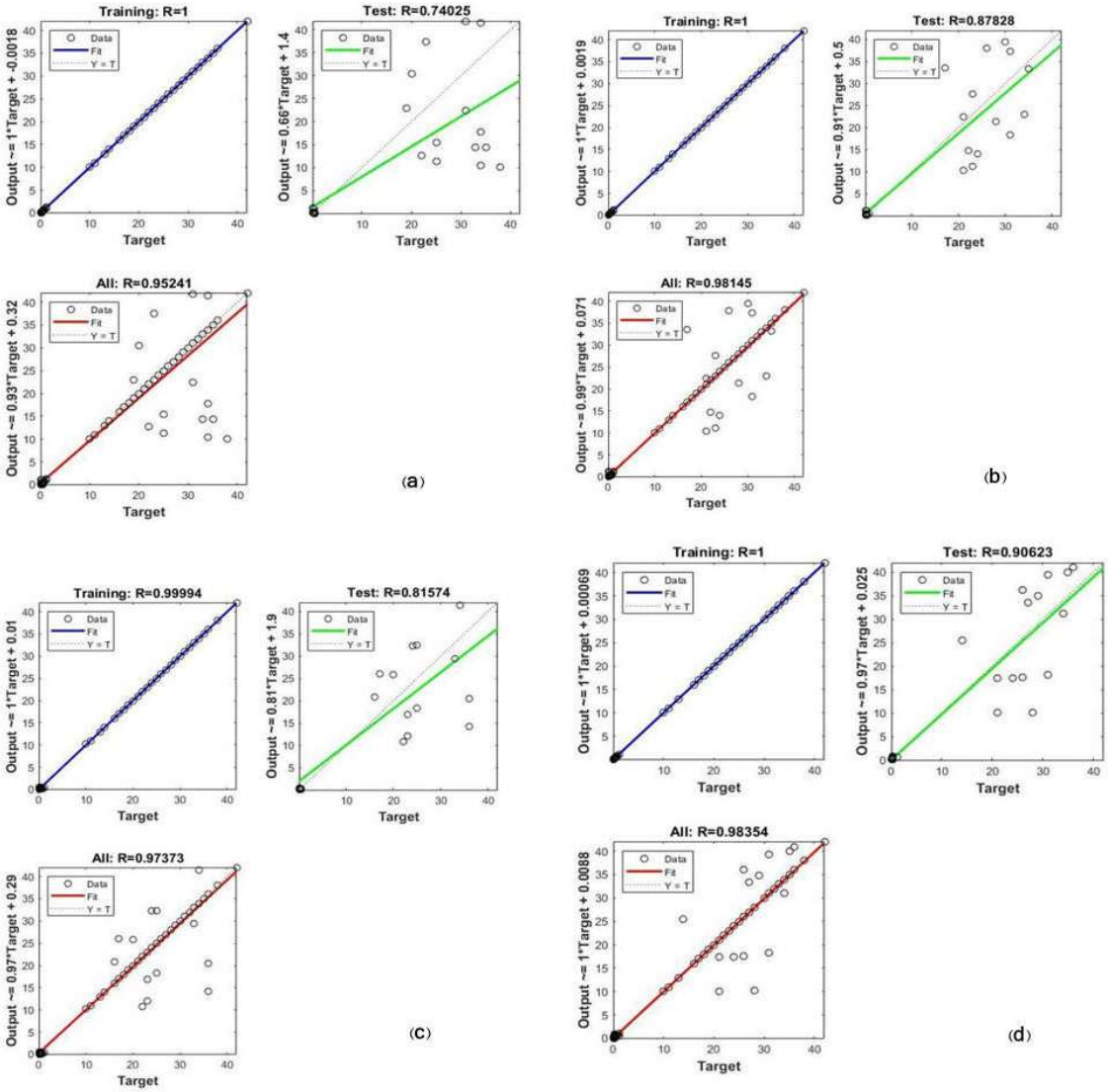

Figure 12. Neural network architectures for the five best-performing configurations (n through r): (a) Network n, (b) Network p, (c) Network q, (d) Network r

Validation of results obtained from artificial neural network

To validate the neural network predictions, the predicted and measured values of internal friction angle and cohesion were compared. Table 8 presents the input parameters for validation samples. The predicted friction angle values from the neural networks and their corresponding experimental measurements are shown in Table 9. Similarly, the predicted cohesion values and experimental measurements are presented in Table 10. Regression analyses between experimental and predicted values were performed for two-layer, three-layer, four-layer, and five-layer configurations for both output parameters (Figures 13 and 14).

As shown in Table 10 and Figure 12, the four-layer neural network achieved the best performance for cohesion prediction with a regression coefficient (R^2) of 0.99. The five-layer configuration provided the second-best results with R^2 of 0.77. For internal friction angle prediction, as indicated in Table 9 and Figure 13, both two-layer and three-layer configurations achieved R^2 of 0.99. According to Table 7, the q-network (four-layer configuration) demonstrated the overall best performance with R values of 1.00 for training, 0.90 for testing, and 0.98 overall.

Table 8. Input parameters of validation samples obtained from laboratory measurements

G_s	%C	%M	%S	%LL	%PL	PI	γ_d(KN/m^3)	%S	AEV	б-Ua(kPa)	USDA
2.66	26	25	49	47	29	18	17.05	16.43	12	200	4
2.71	24	48.5	27.5	25	17	8	18.13	12.97	37	0	8
2.61	39	57	4	42.6	23.7	18.9	16.2	1.34	150	100	3
2.68	29	61	10	31	17.5	13.5	15.5	16.12	43	100	2
2.73	46	44.5	9.5	53.5	32.5	21	14.3	1.25	280	21.6	2
2.72	40	44	16	43.5	23	20.15	13.1	1.11	180	43.3	4
2.64	72	27	1	71	36	35	12.93	14.3	185	120	1
2.66	35	48	17	33	19.4	13.6	17.72	19	55	120	3
2.68	10	37.5	52.5	22	16	6	18.4	14.7	40	50	10
2.66	35	48	17	33	19.4	13.6	17.72	19.0	55	200	3
2.68	10	37.5	52.5	22	16	6	18.4	147.7	40	50	10
2.73	30	42	28	36	17	19	17.7	0.37	40	50	4
2.73	30	42	28	36	17	19	17.7	0.79	40	100	4
2.73	30	42	28	36	17	19	17.7	34.8	40	100	4
2.64	4	11	85	31	17.5	13.5	17.5	34.18	0.7	100	11

Table 9. Comparison of experimental and predicted friction angle values for different network configurations

Results of neural networks					Experiment result
One layer	Two Layers	Three layers	Four Layers	Five Layers	-
16.15	16	16	**16**	16	16
13.08	13	13	**13**	12.99	13
30.04	36	36	**36**	36	36
22.17	18	18	**18**	17.99	18
21.80	14	14	**14**	13.98	14
23.33	28	28	**28**	28	28
34.46	27	27	**27**	27	26.5
21.70	33	33	**33**	33	33
27.21	36	36	**36**	36	36
22.82	28	28	**28**	28	28
30.70	32	32	**35**	32.01	3516
31.15	31	31	**26**	31	26
30.93	28	28	**17**	28	17
28.67	35	35	**25**	34.99	25
22.55	26	26	**35**	26	35

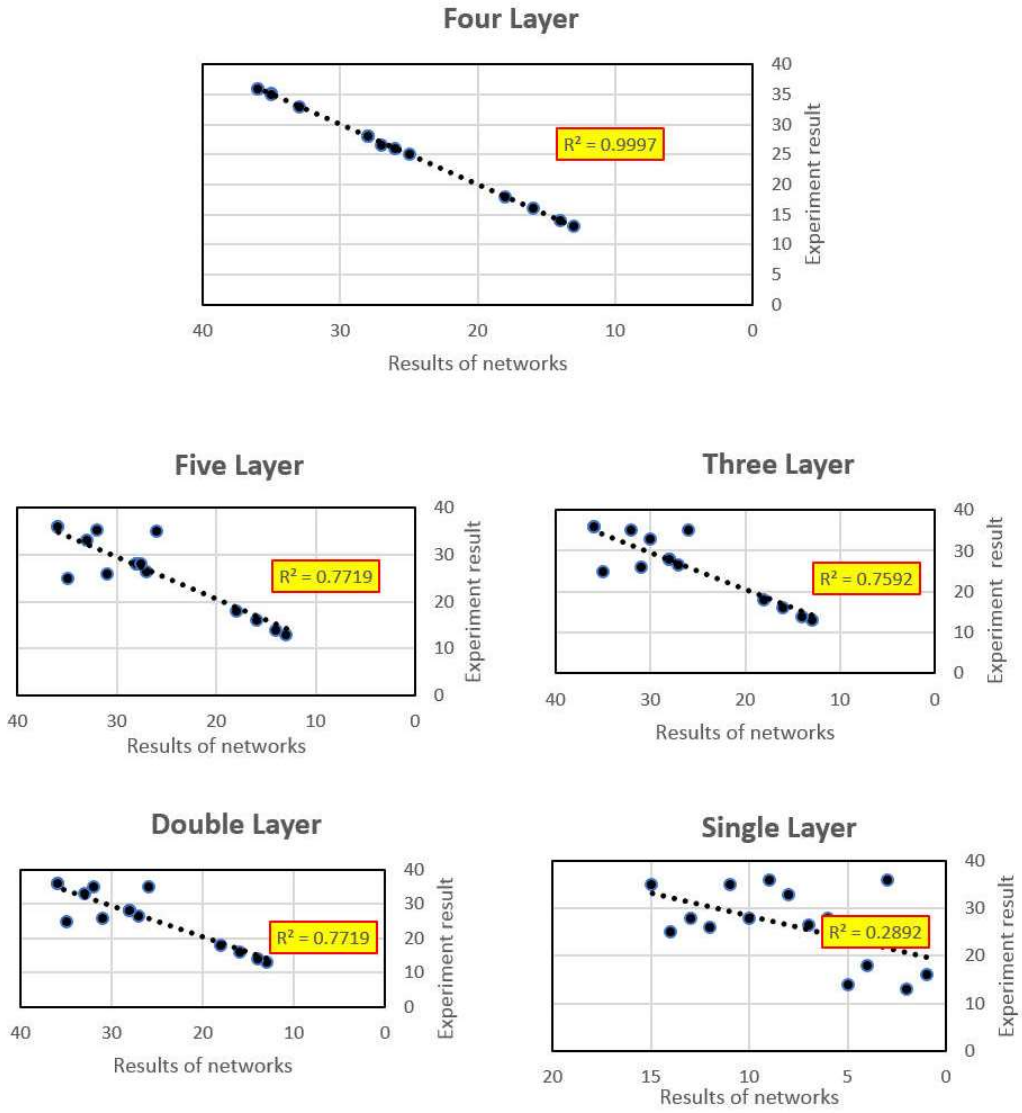

Figure 13. Regression analysis between experimental and predicted friction angle values for two-layer, three-layer, four-layer, and five-layer neural network configurations

Table 10. Comparison of experimental and predicted cohesion values for different network configurations

Results of neural networks					Experiment result
One layer	**Two layers**	**Three layers**	**Four layers**	**Five layers**	**-**
054	0.40	0.44	**0.44**	0.31	0.44
0.50	0.23	0.21	**0.22**	0.28	0.22
051	0.03	0.15	**0.15**	0.21	0.15
0.47	0.17	0.13	**0.13**	0.21	0.13
0.50	0.28	0.43	**0.29**	0.18	0.29
0.49	0.12	0.18	**0.19**	0.21	0.19
0.48	0.17	0.22	**0.24**	0.18	0.24
0.48	0.07	0.17	**0.17**	0.17	0.17
0.47	0.20	0.18	**0.19**	0.18	0.19
0.50	0.27	0.30	**0.29**	0.19	0.29
0.53	0.23	0.23	**0.26**	0.21	0.23
0.46	0.20	0.20	**0.21**	0.22	0.21
0.47	0.17	0.21	**0.22**	0.27	0.22
0.50	0.17	0.21	**0.24**	0.30	0.24
0.53	0.19	0.25	**0.28**	0.23	0.28

To further evaluate the accuracy of the neural network predictions, they were compared with predictions from three established empirical methods: Fredlund et al. (1996), Vanapalli et al. (1996), and Khalili and Khabbaz (1998). The empirical relationships used for these methods are detailed in Table 11. The properties of the soils utilized for this comparison analysis are presented in Table 12. The results demonstrate that the neural network predictions are more accurate than those from these three conventional methods. Furthermore, Figure 15 compares the measured and predicted shear strength values."

Finally, five soil samples were prepared and their input parameters were measured in the laboratory. The shear strength parameters of these soils were then estimated using the neural network and measured experimentally through direct shear testing. The results of this comparison demonstrate that the neural network method can accurately estimate soil shear strength parameters. This validation confirms that the neural network approach can serve as a reliable alternative to time-consuming and expensive laboratory tests. The comparison results are presented in Table 13 and Figures 16, 17, and 18.

Friction angle differences: ranging from 0.2° to 2.6° (percentage differences from 1.01% to 10.97%)

Cohesion differences: ranging from 0.01-0.05 kPa (percentage differences from 3.44% to 14.28%)

Table 12 shows the detailed comparison with the following samples (N1-N5):

Table 11. Empirical Models for Shear Strength Prediction of Unsaturated Soils (Including Key Equations)

Model Reference	Key Equation Form (Approximation)	Key Parameters Used	Notes / Governing Condition
Fredlund et al. (1996)	Concept: $\tau = a_w(u_a - u_w) \times \tan(\Phi')$ (Simplified)	w_a (or a_w), $(u_a - u_w)$, (Suction), Φ'	Extended Form (Eq. 4-5): $\tau_f = c' + (\sigma_n - u_a)\tan\varphi' + (u_a - u_w)[k(\tan\varphi')]$
Vanapalli et al. (1996)	Using θ (Eq. 4-7) $\tau_f = c' + (\sigma_n - u_a)\tan\Phi' + (u_a - u_w) \times [\tan\Phi' (\frac{\theta_w - \theta_r}{\theta_s - \theta_r})]$	θ_w, θ_r (Residual θ), θ_s (Saturated θ)	Using S (Eq. 4-8) $\tau_f = c' + (\sigma_n - u_a)\tan\Phi' + (u_a - u_w) \times [\tan\Phi' (\frac{S - S_\tau}{100 - S_\tau})]$
Khalili & Khabbaz (1998)	Main form (Eq.4-9): $\tau_f = c' + (\sigma_n - u_a)\tan\Phi' + (u_a - u_w)[\chi(\tan\Phi')]$	χ (Parameter linking Suction and AEV)	If AEV < Suction (Eq.4-10): $\chi = [\frac{(u_a - u_w)_{Metric}}{(u_a - u_w)_{AEV}}]^{-0.55}$. If AEV > Suction: $\chi = 0$

Table 12. Soil properties used for comparison with empirical methods

Properties	Soil A	Soil B
Gs	2.72	2.66
%C	42	26
%M	24	25
%S	34	49
%LL	36.4	47
PL	26.4	29
P	10	18
γ_d(KN/m^3)	16.75	17.05
бn-Ua(kPa)	0	200
USCS	2	4
Refrence	(Rahardjo et al., 2004)	(Han et al., 1995)

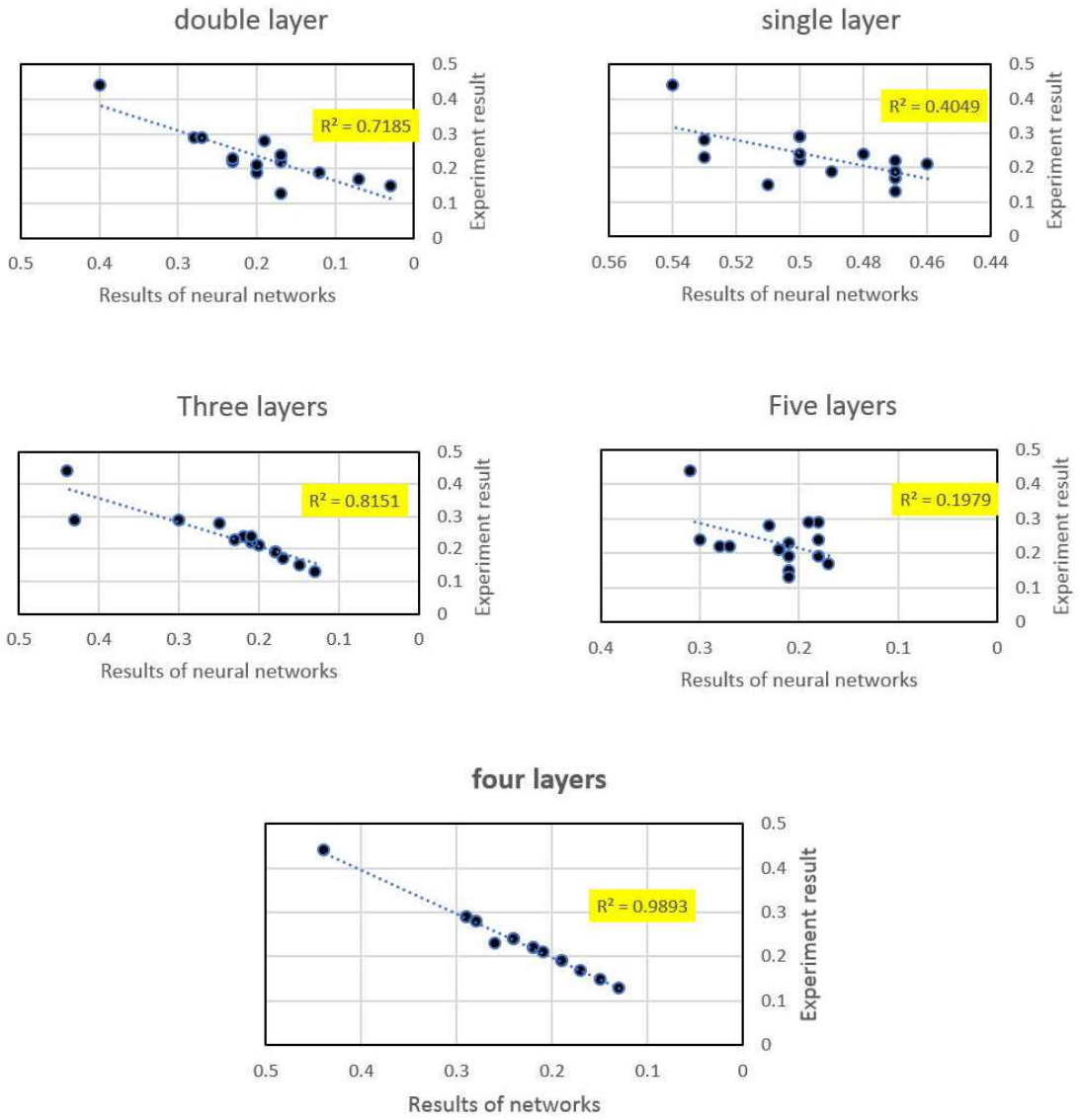

Figure 14. Regression analysis between experimental and predicted cohesion values for two-layer, three-layer, four-layer, and five-layer neural network configurations

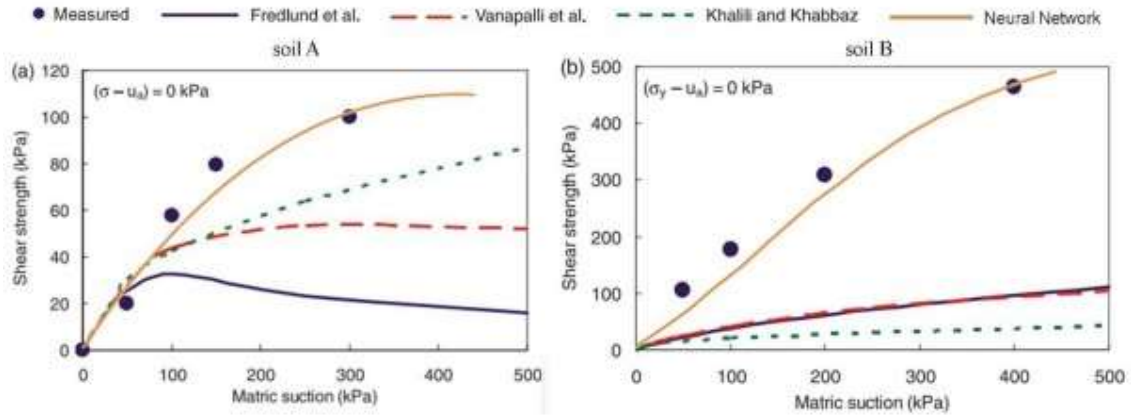

Figure 15. Comparison of measured and predicted shear strength values using empirical methods and the neural network model

Table 13. Comparison of laboratory measurements and neural network predictions for validation samples.

Sample	Laboratory results		Neural network results		Difference in results			
					Cohesion		Internal friction angle	
	Cohesion	Internal friction angle	Cohesion	Internal friction angle	Amount of difference	Percentage difference	Amount of difference	Percentage difference
N1	0.35	19.80	0.30	21	0.05	14.28	0.2	1.01
N2	0.38	37.60	0.33	35	0.05	13.15	2.6	6.91
N3	0.19	31.10	0.20	33	0.01	5.26	2	6.43
N4	0.21	16.40	0.20	18.20	0.01	4.76	1.8	10.97
N5	0.29	29.20	0.30	30	0.01	3.44	0.8	2.73

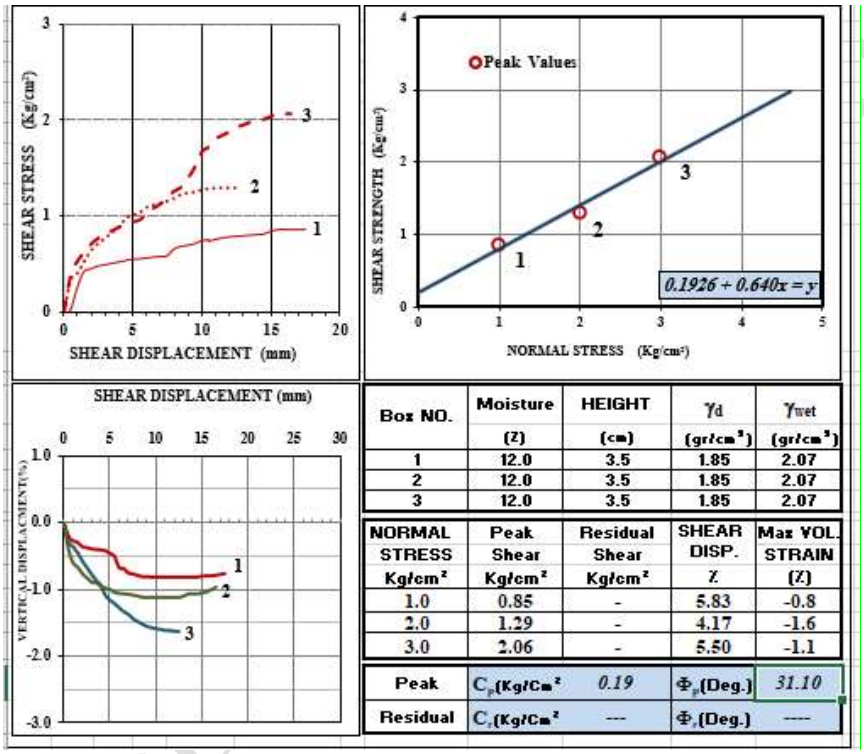

Figure 16. Direct shear test results for sample N3: (top left) shear stress versus shear displacement curves at different normal stresses, (top right) peak shear strength envelope with Mohr-Coulomb failure criterion, (bottom left) vertical displacement versus shear displacement, and (bottom right) summary of test conditions and measured shear strength parameters

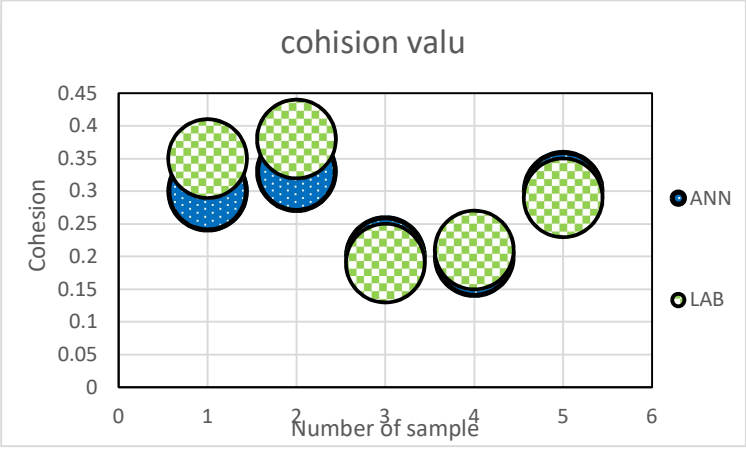

Figure 17. Comparison of laboratory measurements and neural network predictions for cohesion

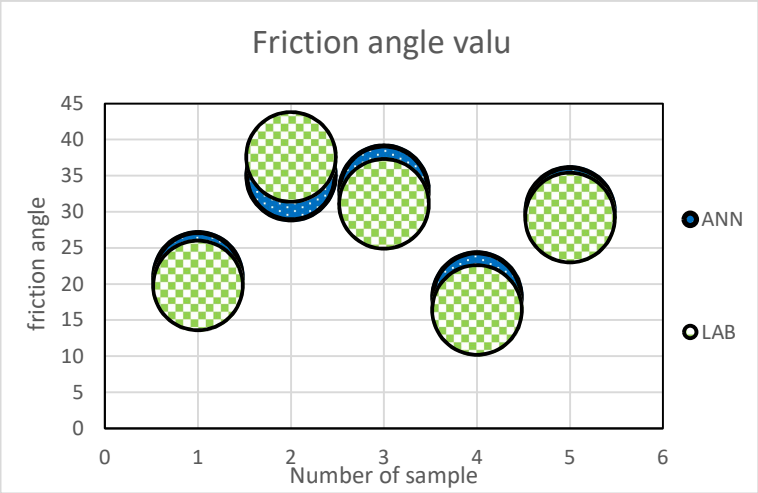

Figure 18. Comparison of laboratory measurements and neural network predictions for friction angle

Conclusion

This study developed and validated an artificial neural network (ANN) model to predict the shear strength parameters of unsaturated soils based on readily available geotechnical properties. A comprehensive evaluation of 195 network configurations led to identifying the optimal architecture and training parameters for this purpose. The four-layer ANN exhibited strong predictive capability for cohesion ($R^2 = 0.99$), followed by the three-layer configuration ($R^2 = 0.98$). For friction angle prediction, several configurations achieved R^2 values up to 0.99, indicating reliable model performance. The optimal combination of the Train BR training function, MSE performance function, and Learn GD adaptive learning algorithm consistently yielded the best outcomes.

Comparative analysis with conventional empirical methods demonstrated that the ANN predictions provided closer agreement with laboratory measurements. The validation using five independent soil samples further supported the practical applicability of the proposed model, indicating that neural networks can be an effective and efficient supplement to conventional testing methods.

Nevertheless, it is acknowledged that the present study is constrained by its dataset size (490 samples) and the range of soil types considered. Hence, the developed model should be viewed as a promising complementary tool rather than a complete substitute for experimental testing. Future research involving a broader spectrum of soil types and larger validation datasets would be valuable to further enhance the generalizability and robustness of the proposed ANN approach.

References

Abd, I. A., Fattah, M. Y., Mekkiyah, H., 2020. Relationship between the matric suction and the shear strength in unsaturated soil. Case Studies in Construction Materials, 13: 00441.

Alzaidy, M. N. J., 2018. A Theoretical Study of Some Unsaturated Properties for Different Soils. Journal of University of Babylon for Engineering Sciences, 26: 149-165.

Bao, C. G., Gong, B. W., Zhan, L. T., 1998. Keynote paper: Properties of unsaturated soils and slope stability for expansive soils. In Proc., 2nd Int. Conf. on Unsaturated Soils, 2: 71-98.

Baziar, M.H., Ghorbani, A., 2005. Evaluation of lateral spreading using artificial neural networks. Soil Dynamics and Earthquake Engineering, 25: 1-9.

Bishop, A. W., Alpan, I., Blight, G. E., Donald, I. B., 1960. Factors controlling the strength of partly saturated cohesive soils.

Chai, J., Khaimook, P., 2020. Prediction of soil-water characteristic curves using basic soil properties. Transportation Geotechnics, 22: 100-295.
Churchland, P. S., Sejnowski, T. J., 1992. The computational brain MIT Press. Cambridge, Massachusetts.
Cunningham, M. R., Ridley, A. M., Dineen, K., Burland, J. B., 2003. The mechanical behaviour of a reconstituted unsaturated silty clay. Géotechnique, 53(2): 183-194.
Das, B. M., 2021. Principles of geotechnical engineering. Cengage Learning.
Fredlund, D. G., 2019. State of practice for use of the soil-water characteristic curve (SWCC) in geotechnical engineering. Canadian Geotechnical Journal, 56(8): 1059-1069.
Fredlund, D. G., Rahardjo, H., 1993. Soil mechanics for unsaturated soils. John Wiley & Sons.
Fredlund, D. G., Xing, A., 1994. Equations for the soil-water characteristic curve. Canadian geotechnical journal, 31(4): 521-532.
Fredlund, D. G., Morgenstern, N. R., Widger, R. A., 1978. The shear strength of unsaturated soils. Canadian geotechnical journal, 15(3): 313-321.
Fredlund, D., Rahardjo, H., Fredlund, M., 2011. Unsaturated soil mechanics in engineering practice: 61.
Gan, J. K. M., Fredlund, D. G., Rahardjo, H., 1988. Determination of the shear strength parameters of an unsaturated soil using the direct shear test. Canadian Geotechnical Journal, 25(3): 500-510.
Gao, Y., Sun, D. A., Zhou, A., Li, J., 2020. Predicting shear strength of unsaturated soils over wide suction range. International Journal of Geomechanics, 20(2): 04019175.
Gao, Y., Sun, D. a., Zhou, A., Li, J., 2020. Predicting shear strength of unsaturated soils over wide suction range. International Journal of Geomechanics.
Garson, G. D. ,1991. A comparison of neural network and expert systems algorithms with common multivariate
Goodfellow, I., Bengio, Y., Courville, A., 2016. Deep learning. MIT press
Goodfellow, I., Bengio, Y., Courville, A., 2016. Deep learning. MIT press.
Guan, G. S., Rahardjo, H., Choon, L. E., 2010. Shear strength equations for unsaturated soil under drying and wetting. Journal of Geotechnical and Geoenvironmental Engineering, 136(4): 594-606.
Hagan M .T., 1995. Neural network design, PWS, USA.
Ho, D. Y., Fredlund, D. G., 1982. A multistage triaxial test for unsaturated soils. Geotechnical Testing Journal, 5(1/2): 18-25.
Huat, B. B., Ali, F. H., Hashim, S., 2007. Relationship between Shear Strength and Soil Water Characteristic Curve of an Unsaturated Granitic Residual Soil. Pertanika Journal of Social Sciences & Humanities, 15:(2).
Ioffe, S., Szegedy, C., 2015. Batch normalization: Accelerating deep network training by reducing internal covariate shift. International conference on machine learning
Johnson, C. E., Grisso, R. D., Nichols, T. A., Bailey, A. C., 1987. Shear measurement for agricultural soils-A review. Transactions of the ASAE, 30(4): 935-0938.
Khaboushan, E. A., Emami, H., Mosaddeghi, M. R., Astaraei, A. R., 2018. Estimation of unsaturated shear strength parameters using easily-available soil properties. Soil and Tillage Research, (184): 118-127.
Khalili, N., Khabbaz, M. H., 1998. A unique relationship for χ for the determination of the shear strength of unsaturated soils. Geotechnique, 48(5): 681-687.
Kim, W. S., Borden, R. H., 2011. Influence of soil type and stress state on predicting shear strength of unsaturated soils using the soil-water characteristic curve. Canadian Geotechnical Journal, 48(12): 1886-1900.
Lee, S. J., Lee, S. R., Kim, Y. S., 2003. An approach to estimate unsaturated shear strength using artificial neural network and hyperbolic formulation. Computers and Geotechnics, 30(6): 489-503.
Likos, W. J., Song, X., Xiao, M., Cerato, A., Lu, N., 2019. Fundamental challenges in unsaturated soil mechanics. Geotechnical fundamentals for addressing new world challenges, 209-236.
Marinho, F. A., & Oliveira, O. M., 2012. Unconfined shear strength of compacted unsaturated plastic soils. Proceedings of the Institution of Civil Engineers-Geotechnical Engineering, 165(2): 97-106.
Myers, N. E., Stokes, M. G., Walther, L., Nobre, A. C., 2014. Oscillatory brain state predicts variability in working memory. Journal of Neuroscience, 34(23): 7735-7743.
Nam, S., Gutierrez, M., Diplas, P., Petrie, J., 2011. Determination of the shear strength of unsaturated soils using the multistage direct shear test. Engineering Geology, 122(3-4): 272-280.

Öberg, A. L., Sällfors, G., 1997. Determination of shear strength parameters of unsaturated silts and sands based on the water retention curve. Geotechnical Testing Journal, 20(1): 40-48.
Oloo, S. Y., Fredlund, D. G., 1996. A method for determination of φ b for statically compacted soils. Canadian Geotechnical Journal, 33(2): 272-280.
Perera, Y. Y., Zapata, C. E., Houston, W. N., Houston, S. L., 2005. Prediction of the soil-water characteristic curve based on grain-size-distribution and index properties. In Advances in pavement engineering : 1-12.
Rahardjo, H., Heng, O. B., Choon, L. E., 2004. Shear strength of a compacted residual soil from consolidated drained and constant water content triaxial tests. Canadian Geotechnical Journal, 41(3): 421-436.
Rassam, D. W., Cook, F., 2002. Predicting the shear strength envelope of unsaturated soils. Geotechnical Testing Journal, 25(2): 215-220.
Rassam, D. W., Williams, D. J., 1999. A relationship describing the shear strength of unsaturated soils. Canadian Geotechnical Journal, 36(2): 363-368.
Rosenblatt, F., 1958. The perceptron: a probabilistic model for information storage and organization in the brain. Psychological review, 65(6): 386.
Russell, S. J., 2010. Artificial intelligence a modern approach. Pearson Education, Inc.
Russell, S. J., 2010. Artificial intelligence a modern approach. Pearson Education, Inc.
Thu, T. M., Rahardjo, H., Leong, E.-C. 2006. Effects of hysteresis on shear strength envelopes from constant water content and consolidated drained triaxial tests. In Unsaturated soils, 1212-1222.
Thu, T. M., Rahardjo, H., Leong, E.-C., 2006. Effects of hysteresis on shear strength envelopes from constant
Thu, T. M., Rahardjo, H., Leong, E.-C., 2007. Critical state behavior of a compacted silt specimen. Soils and foundations, 47(4): 749-755.
Vanapalli, S. K., 2009. Shear strength of unsaturated soils and its applications in geotechnical engineering practice. In Keynote Address. Proc. 4th Asia-Pacific Conf. on Unsaturated Soils. New Castle, Australia, 579-598.
Vanapalli, S. K., Fredlund, D. G., 2000. Comparison of different procedures to predict unsaturated soil shear strength. In Advances in unsaturated geotechnics, pp. 195-209.
Vanapalli, S. K., Fredlund, D. G., Pufahl, D. E., Clifton, A. W., 1996. Model for the prediction of shear strength with respect to soil suction. Canadian geotechnical journal, 33(3): 379-392.
Vanapalli, S., Fredlund, D. 2000b. Comparison of different procedures to predict unsaturated soil shear strength. Geotechnical special publication, 195-209.
Vilar, O. M., 2006. A simplified procedure to estimate the shear strength envelope of unsaturated soils. Canadian Geotechnical Journal, 43(10): 1088-1095.
Water content and consolidated drained triaxial tests. In Unsaturated soils 2006 (pp. 1212-1222).
Wilke, C. O., 2019. Fundamentals of data visualization: a primer on making informative and compelling figures. O'Reilly Media.
Zhang, B., Zhao, Q. G., Horn, R., Baumgartl, T., 2001. Shear strength of surface soil as affected by soil bulk density and soil water content. Soil and Tillage Research, 59(3-4): 97-106.
Zhang, J., Peng, J., Chen, Y., Li, J., Li, F., 2018. Estimation of Soil-Water Characteristic Curve for Cohesive Soils with Methylene Blue Value. Advances in Civil Engineering, 2018(1), 9213674.
Zhou, W. H., Xu, X., Garg, A., 2016. Measurement of unsaturated shear strength parameters of silty sand and its correlation with unconfined compressive strength. Measurement, 93: 351-358.